

Fig. S1 Schematic of CrO<sub>2</sub>-based MTJ with electrodes width of 100  $\mu$ m and the interlayer size of 1 mmx1 mm

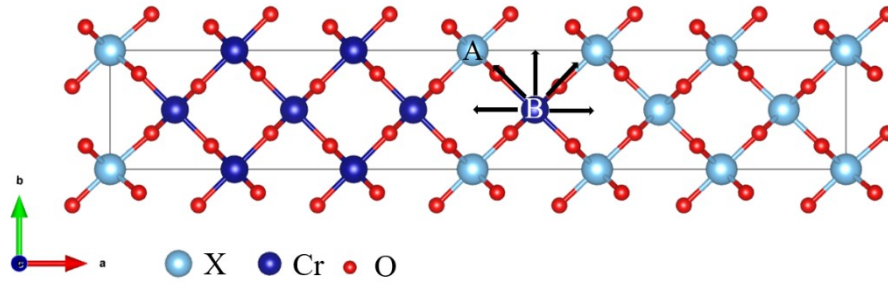


Fig. S2 Model structure of  $\text{CrO}_2/\text{XO}_2/\text{CrO}_2$  ( $X=\text{Ru, Ti, Sn}$ ) MJs with mixed interface for theoretical calculations of spin-polarized quantum transport properties. The arrows indicate magnetic moment orientations of diffused  $\text{Cr}^{4+}$ .

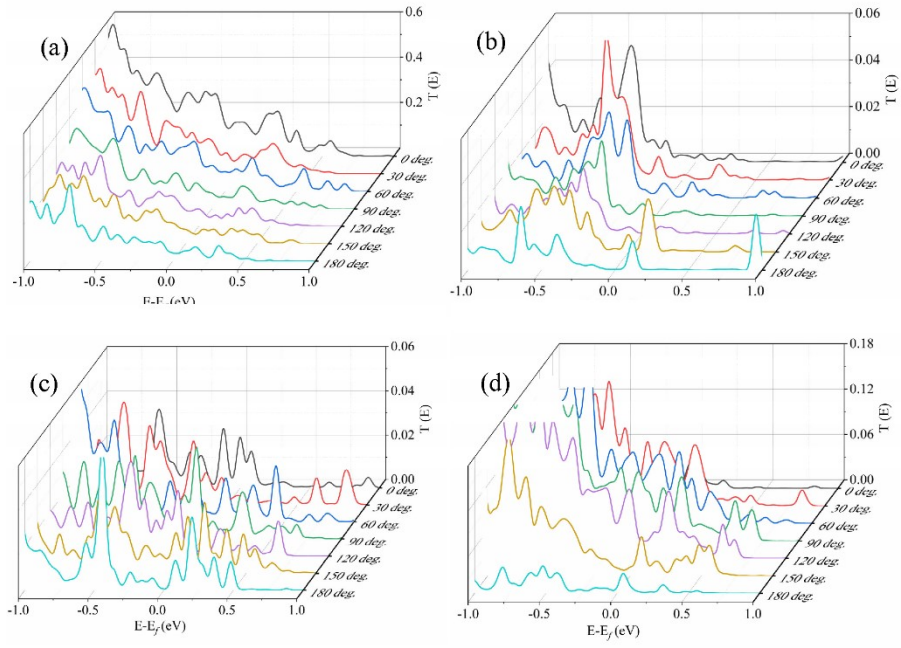


Fig. S3 The transmission coefficients of (a) (c)spin-up and (b) (d) spin-down electrons for  $\text{CrO}_2/\text{RuO}_2/\text{CrO}_2$  MJ dependent on magnetic moment orientation of diffused  $\text{Cr}^{4+}$  for parallel and antiparallel magnetic configurations respectively.

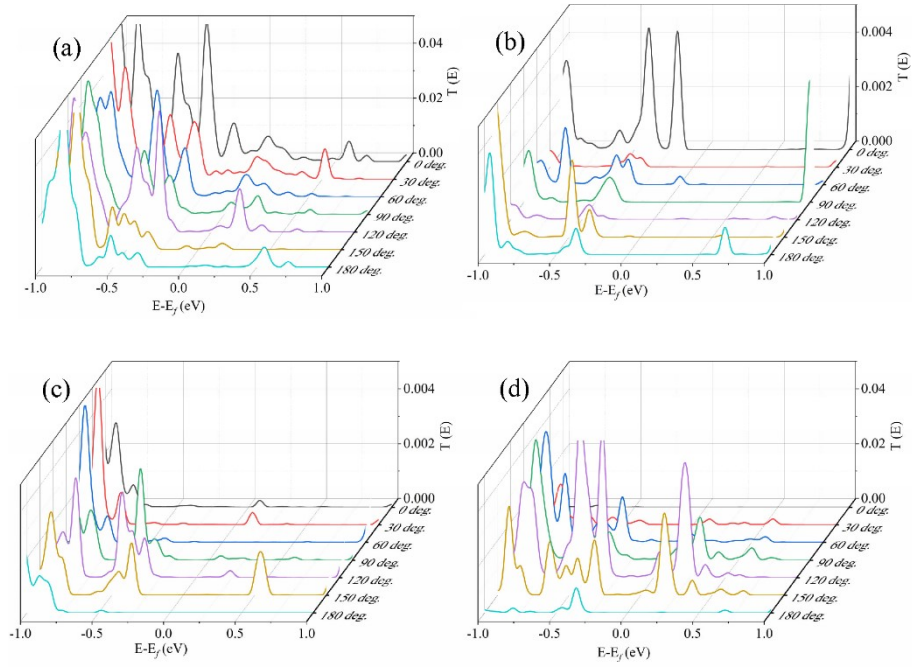


Fig. S4 The transmission coefficients of (a) (c)spin-up and (b) (d) spin-down electrons for  $\text{CrO}_2/\text{TiO}_2/\text{CrO}_2$  MTJ dependent on magnetic moment orientation of diffused  $\text{Cr}^{4+}$  for parallel and antiparallel magnetic configurations respectively.

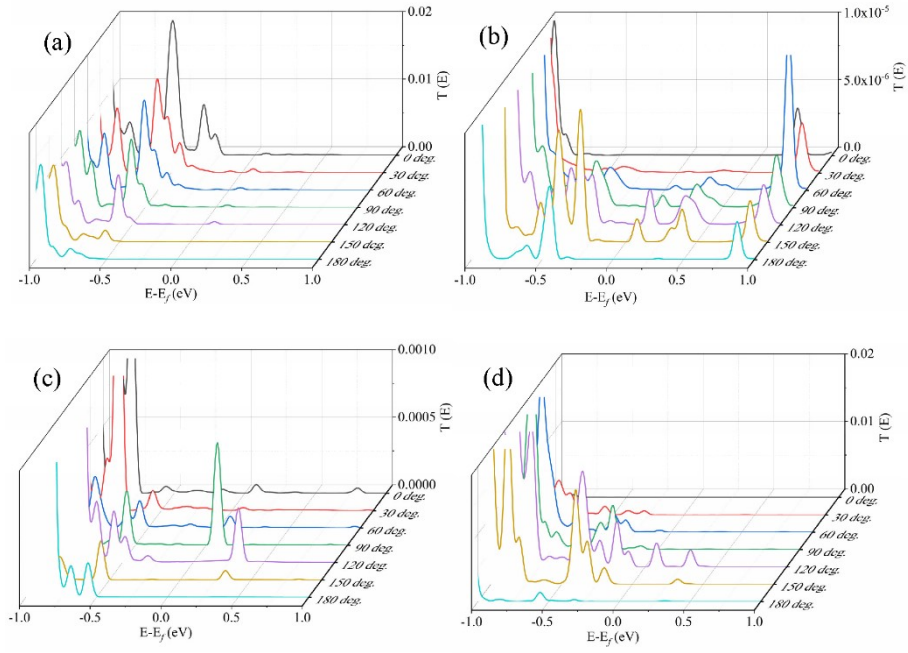


Fig. S5 The transmission coefficients of (a) (c)spin-up and (b) (d) spin-down electrons for  $\text{CrO}_2/\text{SnO}_2/\text{CrO}_2$  MTJ dependent on magnetic moment orientation of diffused  $\text{Cr}^{4+}$  for parallel and antiparallel magnetic configurations respectively.

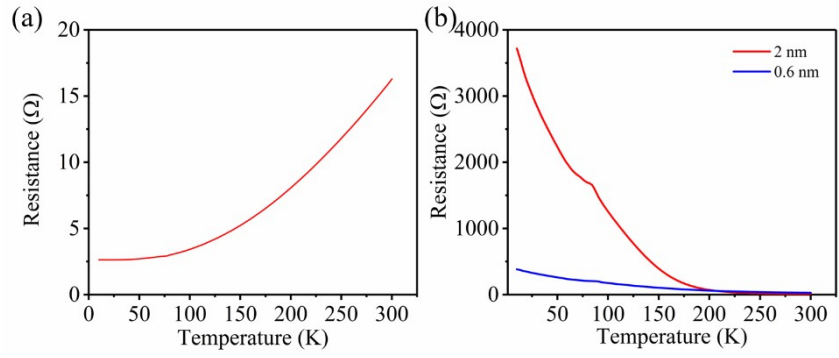


Fig. S6 The temperature dependence of resistance for (a) monolayer CrO<sub>2</sub> film and (b) CrO<sub>2</sub>/TiO<sub>2</sub>/CrO<sub>2</sub> MTJs with TiO<sub>2</sub> tunnel barrier thickness of 0.6 nm and 2 nm.

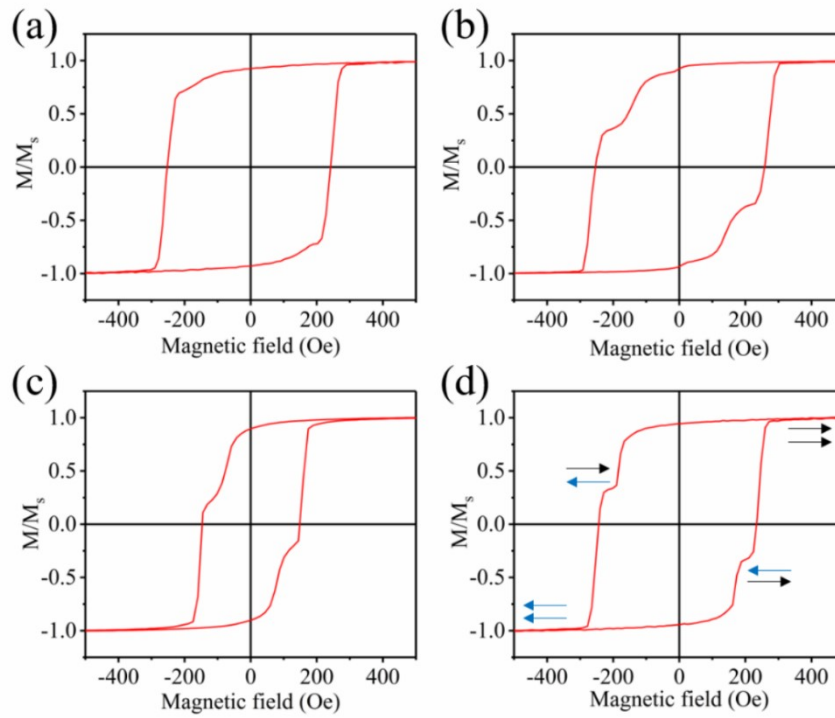


Fig. S7 The normalized hysteresis loops of  $\text{TiO}_2$  (100) substrate /  $\text{CrO}_2$  (40 nm) /  $\text{TiO}_2$  ( $t$ ) /  $\text{CrO}_2$  (12 nm) MTJs with  $\text{TiO}_2$  tunnel barrier thickness ( $t$ ) of (a) 0.6 nm, (b) 1.0 nm, (c) 1.6 nm, (d) 2.0 nm with the external field along  $\text{TiO}_2$  [001] crystal orientation. The arrows in (d) represent the magnetization directions of bottom and top  $\text{CrO}_2$  electrodes.

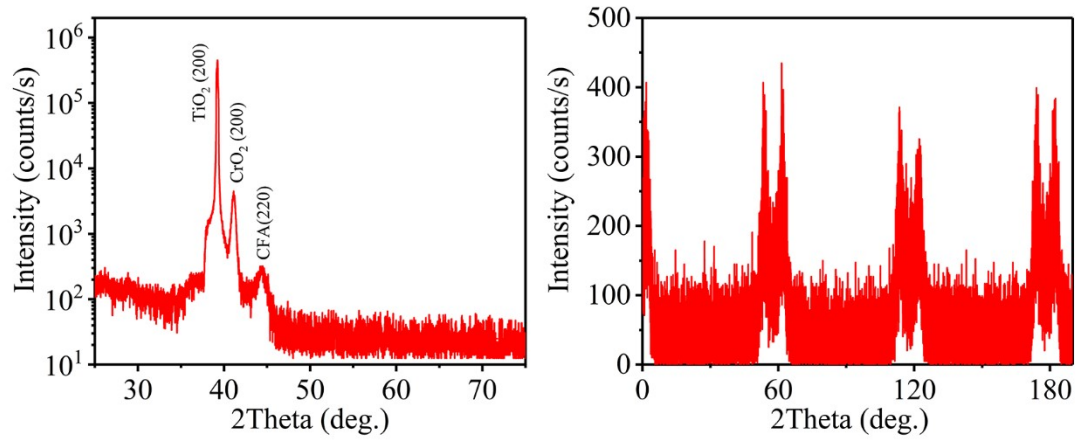


Fig. S8 (a) X-ray diffraction patterns and (b)  $\phi$ -scan of (200) crystal plane of CFA film. XRD pattern and  $\phi$ -scan results verify the epitaxial growth of CFA film.



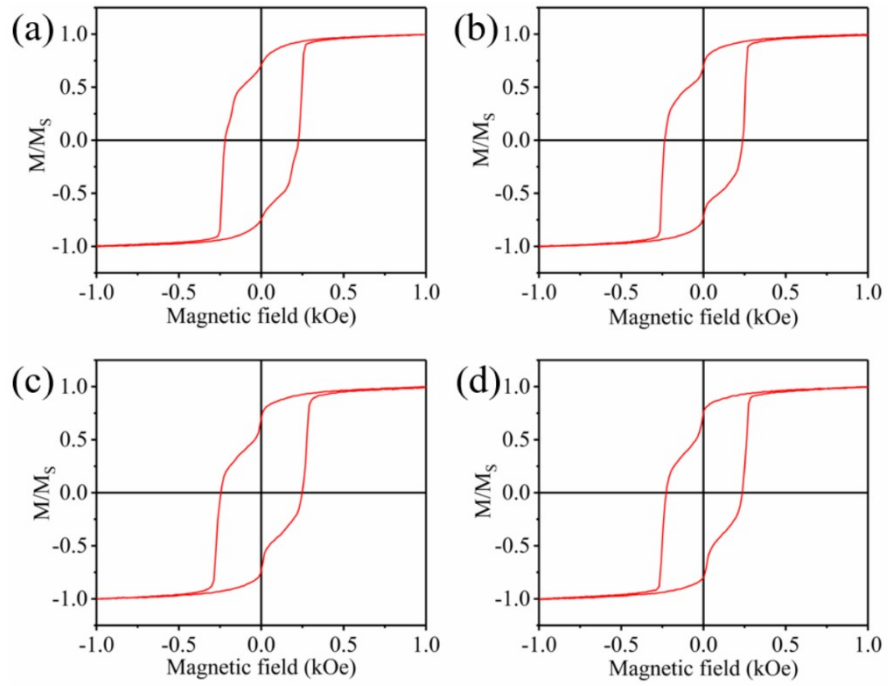


Fig. S9 The normalized hysteresis loops of TiO<sub>2</sub> (100) substrate/ CrO<sub>2</sub> (20 nm) /TiO<sub>2</sub> ( $t$ ) /CFA (5 nm) MTJ with TiO<sub>2</sub> tunnel barrier thickness ( $t$ ) of (a) 0.6 nm, (b) 1.0 nm, (c) 1.6 nm, (d) 2.0 nm with the external field along TiO<sub>2</sub> [001] crystal orientation.

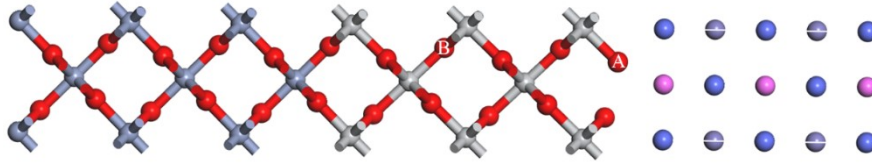


Fig. S10 Model structure of CrO<sub>2</sub>/TiO<sub>2</sub>/CFA MTJ for theoretical calculations of spin-polarized quantum transport properties. The positions labeled as A and B represents the oxygen vacancies located on TiO<sub>2</sub>/CFA interface and inside TiO<sub>2</sub> tunnel barrier respectively.